Journal of Physics and Chemistry of Solids 171 (2022) 111032

Contents lists available at ScienceDirect

Journal of Physics and Chemistry of Solids

journal homepage: www.elsevier.com/locate/jpcs

FLA

Porphyrin based channel for separation of proton isotope: A density functional theory study

Amna Ayub [a], Sehrish Gul [a], Riffat Ayub [b], Zeeshana Bibi [a], Muhammad Ali Hashmi [c], Ahmed Lakhani [d], A. Dahshan [e,f], Khurshid Ayub [g,*], Javed Iqbal [a,h,**]

[a] Department of Chemistry, University of Agriculture, Faisalabad, 38000, Pakistan
[b] Department of Chemistry, University of Wah, Wah Cantt, 47010, Pakistan
[c] Department of Chemistry, Division of Science & Technology, University of Education, 54770, Lahore, Pakistan
[d] Department of Biomedical and Health Sciences, Calumet College of St. Joseph, 2400, New Your Ave, Whiting, IN, 46394, USA
[e] Research Center for Advanced Materials Science (RCAMS), King Khalid University, Abha 61413, P. O. Box, 9004, Saudi Arabia
[f] Physics Department, Faculty of Science, King Khalid University, P. O. Box, 9004, Abha, Saudi Arabia
[g] Department of Chemistry, COMSATS University, Abbottabad Campus, Abbottabad, 22060, Pakistan
[h] Department of Chemistry, College of Science, University of Bahrain, Zallaq, Bahrain

A B S T R A C T

Porphyrin based 2D materials with single atom thickness and uniform pore size have not been explored for the proton isotopes separation. We computationally designed the porphyrin and its derivatives with the doping of oxygen, sulphur and selenium atoms and computed the kinetic energy barrier for H^+, D^+, and T^+ permeation through porphyrin and core modified porphyrins by using M05-2X along with 6-31G (d,p). Zero-point energy is calculated at transition state for H^+ and its other relevant isotopes permeation through porphyrin derivatives. Tunneling ratio of proton isotopes through these 2D structures is calculated by using zero-point energy (ZPE) difference of H^+ to its isotopes. Core modification of porphyrin provides better tunneling ratio for proton isotopes. Among these, mono selenium heteroporphyrin provides the most suitable results. Our study provides the molecular level insight of permeation pathway for proton isotopes through these 2D materials.

1. Introduction

Protonics, a technology concerned with motion of proton in a solid, contribute in energy saving and in conservation of natural environment. Protonic devices play an important role in nuclear reactors, an ultimate source of energy. The working principle of nuclear fusion reactor is utilization of electromotive force or electrochemical proton transport through solid. A fuel cell is another technology where proton have significant role to play. Early in the 19th century, Christian Friedrich, a German physicist made the discovery of the fuel cell for energy conversion [1]. Fuel cells are primarily contain a cathode, an anode, and an electrolyte where the essential component is electrolyte which conduct ions. The electrolyte can be liquid or molten as in phosphoric acid cells and alkaline fuel cells, zinc-air fuel cells, solid oxides fuel cells, and molten carbonate cells where H_3O, OH^-, and CO_3^{2-} are mobile ions in such fuel cells [2]. The majority of mobile electrolyte-based FCs offer high efficiency with high power output, but also have certain drawbacks, including expensive catalysts along with complicated operating conditions, and corrosive electrolytes [3,4]. In order to get over these issues, scientists are moving towards an inexpensive, and ecologically friendly conducting electrolytes to produce energy. Compared to conventional cells, electrochemical cells with proton exchange membranes (PEMs) are a suitable replacement [5,6]. Conducting solid can be a membrane with sufficient pore size, allow transportation of proton through it (see Table 1).

For FCs, PEMs need to have the ideal channel size in order to have higher conductivity and greater selectivity, as well as optimal channel density and homogeneity. Ion bombardment and oxidation, two frequently used techniques for pore drilling and their uniformity have failed in fabrication of exquisite pore channels [7,8]. As the sieving of a proton across the 2-dimensional membrane rely on the membrane's pore diameter along with selectivity, and thickness, certain 2D materials possess homogeneity of pores and excellent conductivity [9–12]. Proton permeate through membrane by exploiting the relative difference of penetration rate or diffusion rate through membrane. Penetration rate or diffusion rate through membrane depend on two Factors, permeance

* Corresponding author.
** Corresponding author.
E-mail addresses: khurshid@cuiatd.edu.pk (K. Ayub), Javed.Iqbal@uaf.edu.pk (J. Iqbal).

https://doi.org/10.1016/j.jpcs.2022.111032
Received 26 July 2022; Received in revised form 7 September 2022; Accepted 30 September 2022
Available online 8 October 2022

Table 1
A & B are the central distance of optimized geometries of porphyrin and its derivatives.

Sr. No		A	B
1.	**Porphyrin**	**NH – NH** 2.17 Å	**N – N** 4.02 Å
2.	**N_3O-porphyrin**	**NH – O** 3.14 Å	**N – N** 4.03 Å
3.	**N_3S-porphyrin**	**NH – S** 2.50 Å	**N – N** 4.41 Å
4.	**N_3Se-porphyrin**	**NH – Se** 2.34 Å	**N – N** 4.51 Å

and selectivity [9–12]. Processing capability of membrane per unit time is called permeance and it is inversely proportional to thickness of membrane. If productivity rate of membrane is high, it means membrane is highly permeable. Furthermore, selectivity is the capability of membrane to separate out desired atom or ion from mixture of any analyte [13]. Ability of each membrane to separate out desired atom/molecule is also dependent on their composition and synthesis process. PEM separation is better approach because of their small foot-print and high – energy efficiency [14,15], That's why PEM is considered as an appealing alternative to other method.

Despite the proton's smaller size compared to other atoms which make easier the passage of proton through membranes, proton isotopes are difficult to separate due to comparable size, shape, electronic properties and even adsorption qualities. The conventional and widespread method is inappropriate for the isotopes permeation since the isolation of atoms is reliant on their size rather than their mass. However, in quantum sieving, separation is based on difference in mass and difference in associated quantum levels of the molecules, confined in pores. Beenakker et al. [16] first proposed his concept and later its effects were studied in several theoretical [16–34] and experimental studies [35–38]. Quantum sieving's effect in the isotope separation was confirmed by the molecular dynamic [18] and experimental [38] studies. Previous research employing kinetic quantum sieving methods demonstrated the advantages of confined potential wells for the separation of H_2/D_2, although potential barriers are thought to be inappropriate for effective isotopologues separation because of their low permeability. However, the quantum tunneling effect starts influencing diffusion behaviors at relatively low temperature when a barrier is evident on the diffusion channel. The heavier isotopes exhibit a significant isotope impact in diffusion at low temperatures as T^+ having a higher diffusion strength than D^+ and H^+.

Bhatia and his co-workers [18], explored the quantum sieving effect for isotopes separation through carbon molecular sieves and zeolites. High efficiency is associated with thickness of membrane, efficiency is high with small thickness. Structure of 2D Nano-porous graphene with 1 atom thickness was firstly provided by Bieri et al. [39]. Three types of membranes, based on carbon are carbon nanotubes (CNTs), carbon membranes and carbon molecular sieving membranes (CMSMs). Nanoporous graphene have been studied as a membrane in experimental studies as well as theoretical studies [14,40–45], but it is very difficult to produce equal sizes of pores in graphene 2-D sheets. Graphene has a range of disadvantages due to its highly challenging pore homogeneity and tunability.

Now a day, many 2-D materials which are based on COFs are synthesized which opened a new door for synthesis of membrane with uniform size pores through bottom up process [46–50]. Porphyrin based 2-D polymeric structure have uniform size pore and near to atomic thickness which is composed of 4 pyrrole rings. Due to uniform combination of pyrrole rings, pore exist in center of porphyrin molecule. Ma and co-worker had designed metal-organic material by using porphyrin as a building block and used for selective uptake CO_2 [51]. In host guest chemistry, cation and anion show interaction with central point or micropore of porphyrin.

One of the stunning method for modification of porphyrin is substitution of pyrrole's nitrogen with one or two hetero-atoms like O, Si, Se, C, S and Te, resulting porphyrin class is known as porphyrinoids or porphyrin containing hetero atoms [52–55]. Although first core modified porphyrin was synthesized in 1970 [56–58] and chemistry of porphyrinoids extended over years and many new porphyrin structure with different substitution were developed. Properties of porphyrinoids were also tuned by substitution.

Porphyrins and its derivatives are used as drug in cancer treatment especially for photodynamic therapy because of its biological importance [59,60]. While some metalloporphyrins are reported in literature as a catalysts for the oxidation of different organic molecules [61]. Expanded porphyrins are reported for separation of CO_2 [62]. Despite all other applications, separation ability of these systems for proton isotope is not documented. Here, mono substituted Porphyrinoids, reported in literature [63] are studied computationally to compare their separation properties for proton isotopes with porphyrin, having 4 pyrrole in structure. The energy curve for protium ion isotopes are computed by density-functional theory to calculate better selectivity.

2. Methodology

At long distance, dispersion forces are important especially when interacting species are neutral and non-polar. In such case, dispersion energy is the only one which responsible for attraction. Commonly used DFT methods like B3LYP are good to predict the geometries and their electronic properties but not valid for study of weak interactions like van der Waals [64]. For study of such systems, long range correlation method should be used, particularly developed by Grimme [65,66] and Truhlar [67–70]. Zhao and Truhlar developed the series of Minnesota functional which describe the "medium range" electron correlation. Compared to the density functionals, M05-2X explains the dispersion interaction of an atom or molecule with a complex and their non-covalent interactions significantly better [71]. M05-2X has been reported in literature for studies of separation of hydrogen [64,72] and helium gas [73] along with proton isotopes separation [74].

Geometrical optimization of porphryrin and its derivative were carried out with Gaussian-09 package, by using global hybrid function called M05-2X along with basis set 6-31G (d,p). All of the calculation were carried out at same level, to make sure that the minima of the obtained structure is without any imaginary frequency.

Furthermore, profile of potential energy was computed to check the impact of porphyrin's pore diameter on adsorption of proton isotopes at different distance. Vibrational frequencies were also computed at same theory level for all the structure to obtain minima at potential energy surface (PES). Energy barrier for H^+, D^+, and T^+ were obtained by passing out proton isotopes through porphyrin and heteroporphyrins at the distance of 3.0 Å to centre. 6-31G(d,p) basis set was used for scanning the path of porphyrin and porphyrin analogues to protium ion isotopes.

3. Result and discussion

As we optimized the geometries of porphyrin and its derivatives to local minima, we noticed that substitution of hetero-atom changed the pore diameter of porphyrin. Changes occur in diameter of pore which may alter the potential energy barrier for proton isotopes. Pristne porphyrin exhibited distance of 2.057 Å for NH - NH and 4.288 Å for N – N, respectively in the centre of ring as shown in Fig. 1.

After optimization, porphyrin and its derivatives are optimized to a stable ground state which gives on to reasonable increase in core diameter of porphyrin. Reasons for this increase are, changing in bond length of especially central doped hetero atom as well as replacement of NH with hetero atom, as pure porphyrin have NH-NH while heteroporphyrin have NH-X (X can be oxygen, sulphur, selenium). Periodic trend of doped atoms in group 7B is like that sulphur and selenium are

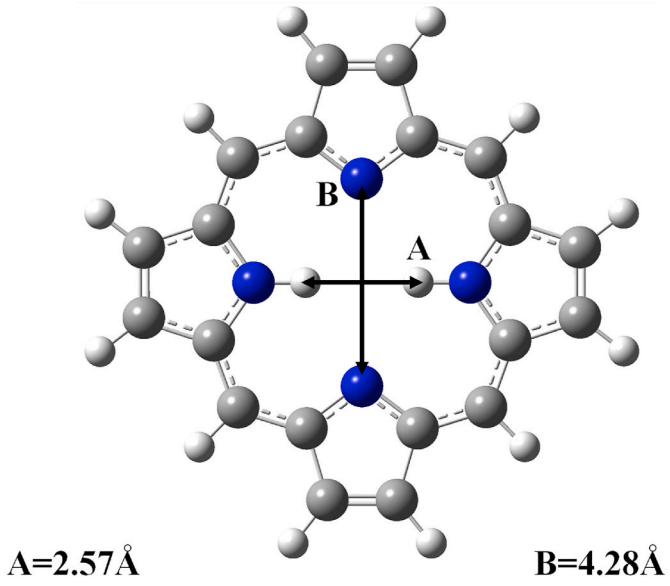

Fig. 1. Structure of porphyrin with the labelling A and B. **A** represent the distance between two hydrogen of pyrrole ring and **B** represent the distance between two nitrogens toward centre of pyrrole ring.

placed below the oxygen and size trend among these atoms is O > S > Se. Among these derivatives, increase of internal diameter is directly proportional to periodic trend as nitrogen shown slighter change in comparison to sulphur and selenium. Oxygen and nitrogen belong to same period in periodic table, so having no such difference of size but sulphur and selenium doped shown much deviation towards increase in diameter because of their size increase. When size of doped atom increase, it expands ring by changing bond length of adjacent atoms to adjust itself inside the ring which results in increase of internal diameter of membrane.

3.1. Separation path of protium isotope through porphyrin

Pure porphyrin is composed of four pyrrole rings, bonded to one another in such a way that leads to a reasonable diameter in their centre. Proton starts to travel from distance of 3.0 Å perpendicular to centre of porphyrin ring as shown in Fig. S1.

When proton moves toward centre, the energy start to reduce frequently up to the distance of 1 Å. At this point, minimum on the PES is observed. After that point, energy gradually increases. The maximum of the potential energy surface is observed at 0 Å. Observed Energy maxima is due to interaction between H^+ and centre of ring. At center of ring, the distance between two hydrogen atoms in pyrrole ring's centre is approximately 2.16 Å as shown in Fig. S2, which hindered permeating ion because of electronic attraction. Due to this, energy barrier at this point for H^+ is 17 kcal/mol which is 0.73 eV as shown in Fig. 2a.

Proton permeation via graphene by implementation of method CI-NEB method as already reported in literature, provided ≈2.21 eV (50 kcal/mol) of the penetration barrier [75]. While, 1.48 eV (34 kcal/mol) and 1.04 eV (23.98 kcal/mol) energy barrier are noted by using of MP2 method on *graphene* and *h-BN fragment*, respectively [76]. This comparison shows that porphyrin have lower energy barrier for proton as compared to *h-BN fragment* and *graphene* by difference of 0.31 eV and 0.75 eV. Both the chemisorption and physiosorption methods implemented on graphene and *h-BN fragment* for proton permeation study have been reported in literature [77]. Reported energy barrier for proton permeation through graphene via chemisorption and physiosorption penetration are approximately 3.5–4 eV and 1.4–2.6 eV, respectively [75,78,79] whereas physisorption of proton on graphene sheet have smaller barrier than chemisorption [75,78,79]. The ZPE difference of proton isotopes through porphyrin is smaller as compared to *h-BN fragment* and graphene either through chemisorption or physisorption. This difference in energy barrier is due to proton interaction with central atoms in ring and secondly due to pore size. If pore diameter of membrane is smaller as compared to permeating ion, permeating ion suffer with high energy barrier.

Separation of protium isotopes via conventionally used membrane is a challenging process. Geim and co-worker reported that protium isotopes separation is achievable through 2-D graphene sheet, due to their velocity difference when they permeate through membrane with isotope dependent velocity [80]. According to Geim and co-worker, the quantum zero-point vibrations difference is because of difference in isotope dependent velocity. For quantitative model verification we computed the ZP energy. DFT calculation shown the trend of ZPE for the isotopes of protium ion i.e., $ZPE(^{+}_{H}) > ZPE(^{+}_{D}) > ZPE\ (^{+}_{T})$. The calculated difference of ZPE ratio of H^+/D^+ and H^+/T^+ are −0.25 kcal/mol and −0.35 kcal/mol, respectively, which are ≈ −0.01eV and −0.015 eV as shown in Fig. 2b. The ZPE difference $ZPE(^{+}_{H})/ZPE(^{+}_{D})$ and $ZPE(^{+}_{H})/ZPE(^{+}_{T})$ through graphene are 0.06eV and 0.09eV, respectively [76] which are equal to 1.38 kcal/mol and 2.07 kcal/mol.

Arrhenius equation $k_1/k_2 = e^{-\Delta Ea/RT}$ is used to calculate the ratio of tunneling reaction constant. R is universal gas constant while T measure

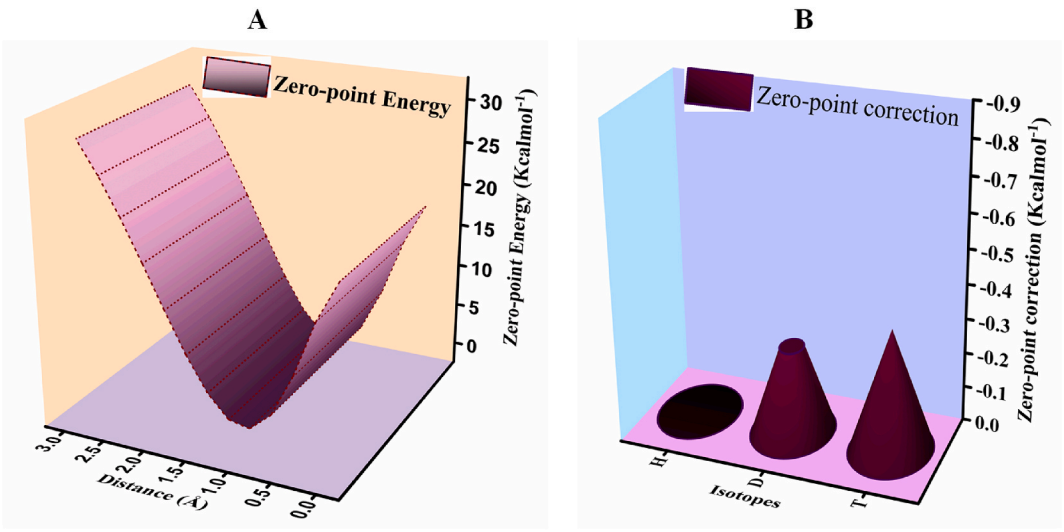

Fig. 2. (a) PE surface for scan of proton through porphyrin **(b)** ZPE difference for H^+ over D^+ and H^+ over T^+.

in kelvin and ΔEa is activation energy difference between two reactants. By assuming that ZPE can lower the activation energy barrier, we computed the activation barrier difference from ZPE difference for proton isotopes, i.e, $\Delta E_{H+/D+} = -0.25$ kcal/mol and $\Delta E_{H+/T+} = -0.35115$ kcal/mol. By using Arrhenius equation, tunneling ratio observed for H^+/D^+ and H^+/T^+ are 1.57 and 1.87, respectively. The difference of permeation velocities for proton isotopes is because of difference in zero-point tunnelling ratio. Higher difference of tunnelling ratio indicate the easy separation of proton isotopes in relevancy to each other because this ratio is based on potential energy barrier which they faced during permeation through membrane or sheet. Lighter elements liken H^+ moves faster through sheet rather than heavier isotopes D^+ and T^+. The tunnelling ratio difference above 1 is enough to get separate the proton from its isotopes.

3.2. Separation path of protium isotope through mono-sulphur heteroporphyrin

Mono sulphur heteroporphyrin contains one sulphur instead of a nitrogen as shown in Fig. S3. For pure porphyrin, NH-NH distance is 2.057 Å whereas it increased up to to 3.057 Å for S-porphyrin. Reason for this increase in size of pore is removal of hydrogen atom at the position of sulphur atom due to its satisfied oxidation state.

When proton start to travel perpendicularly from distance of 3 Å towards centre, the energy gradually decreases up to the distance of 1 Å and energy minima is observed at this point but after this, energy start to increase gradually when it moves towards centre of the ring. The energy barrier observed through mono-S porphyrin for proton permeation is ≈ 12.6 kcal/mol (Fig. 3a), about 5 kcal/mol lower than porphyrin. Observed energy maxima at PE surface is smaller in comparison to graphene and *h-BN fragment* with the difference of 21.4 kcal/mol and 11.38 kcal/mol respectively [76]. This energy barrier difference of graphene and *h-BN fragment* to S-porphyrin is much higher as graphene pore diameter is smaller than S-porphyrin. But in comparison to pure porphyrin, the energy barrier of m-sulphur heteroporphyrin is smaller by the difference of 4.4 kcal/mol, the reason for this small difference is diameter change by doping of sulphur in place of nitrogen. By doping of sulphur, pore size increase by the difference of 1 Å, as their pore size from the side of NH – NH and NH – S are 2.057 Å and 3.057 Å respectively as shown in Fig. S3. Due to larger pore size, proton suffer less hindrance when permeate through m-Sulphur porphyrin. Secondly larger distance of 1.49 Å between H^+ and S atom as shown in Fig. S4, reduce the chances of proton interaction with lone pair of sulphur.

In Arrhenius equation, for calculating tunneling ration zero-point energy difference between isotopes can be used as activation energy difference $\Delta E_{H+/D+}$ and $\Delta E_{H+/T+}$. Observed values of $ZPE(^{\ddagger}_{H})$ - $ZPE(^{\ddagger}_{D})$ and $ZPE(^{\ddagger}_{H})$ - $ZPE(^{\ddagger}_{T})$ are −0.75 kcal/mol and −0.8 kcal/mol which are smaller than values of porphyrin for H^+/D^+ and H^+/T^+. Lower values of $ZPE(^{\ddagger}_{H})/ZPE(^{\ddagger}_{D})$ and $ZPE(^{\ddagger}_{H})/ZPE(^{\ddagger}_{T})$ for m-S porphyrin indicate the easily separation of proton from its isotopes due to noticeable difference in their tunnelling ratio. The computed tunneling ratio constant for H^+/D^+ and H^+/T^+ are 3.84 and 4.31 as shown in Fig. 3b. Tunneling ratio of mono-sulphur heteroporphyin is higher to pure porphyrin.$^+$

3.3. Separation path of protium isotope through mono-selenium heteroporphyrin

Structure of mono-selenium heteroporphyrin is almost similar to m-S heteroporphyrin but pore size reduced by selenium doping because selenium is bigger in size. When selenium atom doped in porphyrin, it repels surrounding pyrrole rings to adjust itself in porphyrin centre because its size is almost 1.6 times greater to nitrogen as structure shown in Fig. S5.

In optimized structure, distance between NH-Se is 2.34 Å whereas NH-NH and NH-S shown 2.057 Å and 3.057 Å respectively. Although NH-Se distance is smaller than NH-S but still larger to NH-NH. But distance between N-N in mono-selenium doped is 4.5 Å which is greater to pure porphyin and mono sulphur doped. Reason for this larger distance is size difference of selenium to other atoms which adjust by repelling away surrounding rings.

As H^+ directed towards centre of ring, low energy structure is observed at 1 Å distance. While at 0 Å, it bears a strong energy barrier of about 50.33 kcal/mol as shown in Fig. 4a. Energy barrier of under study derivative is greater than previously discussed porphyrin and its S doped derivative while almost equal to graphene which is studied through CI-NEB by Meng Miao and his group [75]. At 0 Å, in the centre of the ring, distance of permeating protium ion to heteroselenium atom is about 1.22 Å and 1.12 Å to NH as shown in Fig. S6. Larger size of selenium hindered the permeation of proton ion through membrane's centre and results in higher energy barrier relative to other porphyrin derivatives.

The observed values of $ZPE(^{\ddagger}_{H})/ZPE(^{\ddagger}_{D})$ and $ZPE(^{\ddagger}_{H})/ZPE(^{\ddagger}_{T})$ are −0.02 kcal/mol and −0.03 kcal/mol as shown in Fig. 4b. As the difference of ≈0.23 kcal/mol, and 0.32 kcal/mol for porphyrin and 0.73 kcal/mol and 0.78 kcal/mol for m-S heteroporphyrin, the ZPE difference of H^+/D^+ and H^+/T^+ for m-Se heteroporphyrin is much smaller than pure porphyrin and m-sulphur porphyrin. By using ZPE difference values, calculated tunnelling ratio of proton isotopes through this under study porphyrin derivative are 1.03 and 1.05 respectively. Small difference between tunnelling ratio for deuterium and tritium ion made it difficult to separate proton isotopes. Although, H^+ faced high energy barrier of about 50 kcal/mol while permeating through mono selenium heteroporphyrin which is feasible for protium ion separation. But

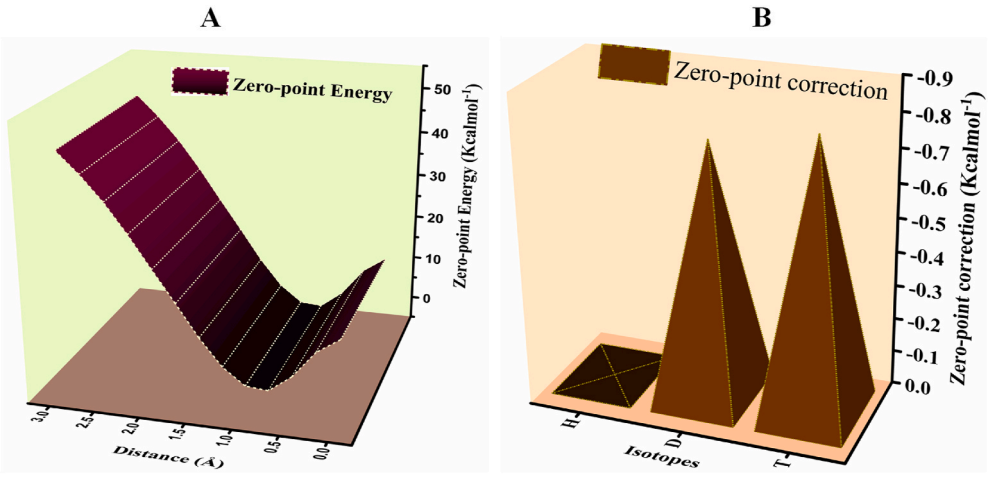

Fig. 3. **(a)** Calculated PE surface for proton through m-sulphur porphyrin **(b)** ZPE corrections of H^+/D^+ and H^+/T^+.

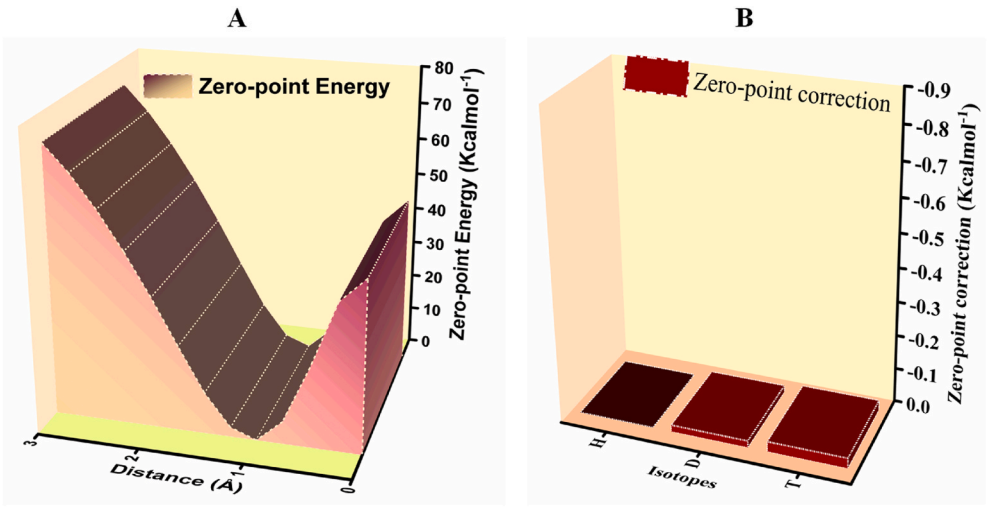

Fig. 4. **(a)** TS of m-selenium porphyrin at distance of 0 Å with energy barrier of 50 kcal/mol **(b)** Zero-point energy correction of H^+ to D^+ and T^+.

difference between ZPE ratio of H^+/D^+ and H^+/T^+ is much smaller which is about 0.01 kcal/mol which leads to smaller difference between tunnelling ratios. This smaller difference of ZPE ratio of selenium heteroporphyrin reduced its efficiency for H^+ isotopes separation in relevancy to porphyrin and mono sulphur heteroporphyrin.

3.4. Separation path of protium isotope through m-oxygen heteroporphyrin

Oxygen is substituted in place of NH in porphyrin structure to evaluate its selectivity for proton and its isotopes, either it's well suited for proton permeation or not. As size of oxygen is smaller than nitrogen, by periodic manners but not more than sulphur and selenium. So, central pore size from NH to O increase up to 3.14 Å while pore sizes of NH-Se and NH-S are 2.34 Å and 3.057 Å as shown in Fig. S7, but distance between N-N is 4.03 Å, smaller than other porphyrin derivatives.

In the case of mono oxygen heteroporphyrin, a minima for protium ion wih porphyrin is located at distance of 0.5 Å from sheet's centre. Energy minima for m-oxygen heteroporphyrin is located at 0.5 Å while for porphyrin and its derivatives is located at different distance toward centre of ring. At the distance of 0 Å, H^+ bear barrier of 0.62 kcal/mol as shown in Fig. 5a. The distance of H^+ to nearest atom (hydrogen) in centre of ring is almost 1.05 Å and distance to oxygen atom in ring is almost 2.08 Å as shown in Fig. S8. The variation of this distance of H^+ is due to variation of their bond length. This derivative has lowest PE surface value for proton permeation among graphene, *h-BN fragment*, pure porphyrin, and its derivatives. Among all the derivatives, oxygen dopant have smallest size and provides larger diameter. Lowest energy barrier through this derivative is because of larger diameter which is approximately 4.16 Å (see Fig. 6).

Observed values of ZPE(^+_H) - ZPE(^+_D) and ZPE(^+_H) - ZPE(^+_T) are −0.265 kcal/mol and −0.357 kcal/mol as shown in Fig. 5b. Values of ZPE(^+_H)/ZPE(^+_D) and ZPE(^+_H)/ZPE(^+_T) for m-oxygen heteroporphyrin are almost equal to pure porphyrin but higher than other porphyrin derivatives. The tunnelling ratio for deuterium and tritium ion are approx. 1.56 and 1.82. Tunnelling ratio of understudy porphyrin's derivative and porphyrin is almost equal because as we discussed that value of ZPE for D^+ and T^+ through m-nitrogen heteroporphyrin is almost equal to pure porphyrin. While too much smaller in comparison to mono-sulphur heteroporphyrin.

4. Conclusion

We computed the energy barrier for proton and its isotopes by using M05-2Xm method along 6-31G(d,p) basis set. We studied the movement of protium isotopes through porphyrin ring and its derivatives. Lowest energy structure for protium ion with porphyrin is located at the distance of 1 Å perpendicularly to porphyrin and its derivatives except m-

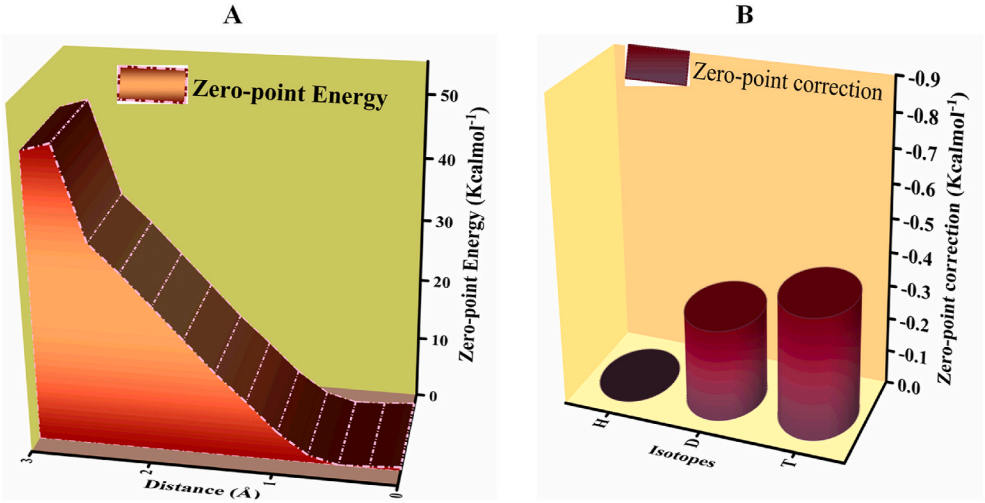

Fig. 5. **(a)** Pathway scan of protium ion through m-oxygen porphyrin **(b)** ZPE correction of H^+ to D^+ and T^+.

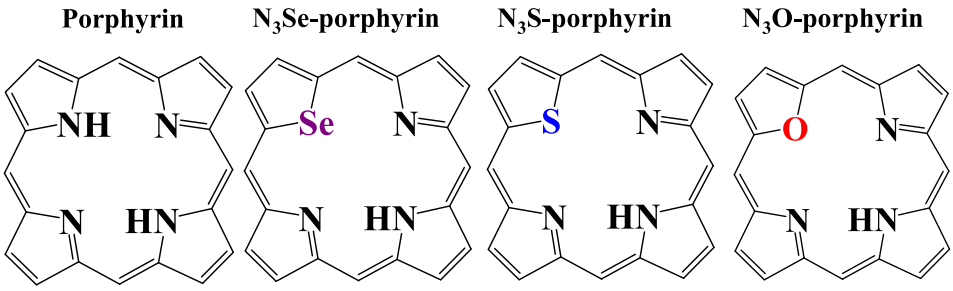

Chart 1. Different structures of Porphyrin with hetero-atom substitution.

oxygen porphyrin it is 0.5 Å. Reason for this difference of energy minima point is presence of lone pair on oxygen which attract the electron deficient H^+ isotopes at shorter distance. At PE surface, m-selenium have highest energy barrier for proton permeation among studied hetero-porphyrins which is about 50 kcal/mol and it also have lowest tunnelling ratio for H^+/D^+ and H^+/T^+ i-e., about 1.03 and 1.05 respectively. This tunnelling ratio and high energy barrier make it unsuitable for isotopes separation. While nitrogen provided the lowest energy barrier for proton and its isotopes but didn't provide the best fitted tunnelling ratio. Tunnelling ratio observed through m-oxygen heteroporphyrin and pure porphyrin are almost equal i.e, 1.57 and 1.87 for D^+ and T^+. Although m-sulphur have energy barrier of almost 12.6 kcal/mol but provided lowerest values of ZPE as, −0.75 kcal/mol and −0.814 kcal/mol for deuterium and tritium respectively as compared to other hetero porphyrins and have highest H^+/D^+ and H^+/T^+ separation ratio among other hetero porphyrins which is about 3.5 and 4.

Author agreement

The Authors declare no conflict of interest.

Declaration of competing interest

The authors declare that they have no known competing financial interests or personal relationships that could have appeared to influence the work reported in this paper.

Data availability

Data will be made available on request.

Acknowledgement

The authors are acknowledged for the technical support from Punjab Bio-energy Institute, University of Agriculture, Faisalabad, Pakistan. We also thank for the support by the King Khalid University through a grant RCAMS/KKU/03-22 under the Research Center for Advance Materials (RCAMS) at King Khalid University, Saudi Arabia.

Appendix A. Supplementary data

Supplementary data to this article can be found online at https://doi.org/10.1016/j.jpcs.2022.111032.

References

[1] M. Grote, Surfaces of action: cells and membranes in electrochemistry and the life sciences, Stud. Hist. Philos. Sci. C Stud. Hist. Philos. Biol. Biomed. Sci. 41 (2010) 183–193.
[2] M. Rahimnejad, G. Najafpour, Microbial fuel cells: a new source of power, Biochem. Eng. Biotechnol. (2011) 1–31.
[3] I. Palmer, C.M. Seymour, R.A. Dams, Application of Fuel Cells to Power Generation Systems, Google Patents, 1995.
[4] J. Selman, Research, Development, and Demonstration of Molten Carbonate Fuel Cell Systems, Fuel cell systems, Springer1993, pp. 345-463.
[5] O.Z. Sharaf, M.F. Orhan, An overview of fuel cell technology: fundamentals and applications, Renew. Sustain. Energy Rev. 32 (2014) 810–853.
[6] K. Pourzare, Y. Mansourpanah, S. Farhadi, Advanced nanocomposite membranes for fuel cell applications: a comprehensive review, Biofuel Res. J. 3 (2016) 496–513.
[7] S.C. O'Hern, M.S. Boutilier, J.-C. Idrobo, Y. Song, J. Kong, T. Laoui, M. Atieh, R. Karnik, Selective ionic transport through tunable subnanometer pores in single-layer graphene membranes, Nano Lett. 14 (2014) 1234–1241.
[8] K. Yoon, A. Rahnamoun, J.L. Swett, V. Iberi, D.A. Cullen, I.V. Vlassiouk, A. Belianinov, S. Jesse, X. Sang, O.S. Ovchinnikova, Atomistic-scale simulations of defect formation in graphene under noble gas ion irradiation, ACS Nano 10 (2016) 8376–8384.
[9] M. Carta, R. Malpass-Evans, M. Croad, Y. Rogan, J.C. Jansen, P. Bernardo, F. Bazzarelli, N.B. McKeown, An efficient polymer molecular sieve for membrane gas separations, Science 339 (2013) 303–307.
[10] X. Zhu, C. Tian, S. Chai, K. Nelson, K.S. Han, E.W. Hagaman, G.M. Veith, S. M. Mahurin, H. Liu, S. Dai, New tricks for old molecules: development and application of porous N-doped, carbonaceous membranes for CO2 separation, Adv. Mater. 25 (2013) 4152–4158.
[11] Y. Peng, Y. Li, Y. Ban, H. Jin, W. Jiao, X. Liu, W. Yang, Metal-organic framework nanosheets as building blocks for molecular sieving membranes, Science 346 (2014) 1356–1359.
[12] H. Guo, W. Zhang, N. Lu, Z. Zhuo, X.C. Zeng, X. Wu, J. Yang, CO2 capture on h-BN sheet with high selectivity controlled by external electric field, J. Phys. Chem. C 119 (2015) 6912–6917.
[13] Y. Jiao, A. Du, M. Hankel, S.C. Smith, Modelling carbon membranes for gas and isotope separation, Phys. Chem. Chem. Phys. 15 (2013) 4832–4843.
[14] D.-e. Jiang, V.R. Cooper, S. Dai, Porous graphene as the ultimate membrane for gas separation, Nano Lett. 9 (2009) 4019–4024.
[15] D.L. Gin, R.D. Noble, Designing the next generation of chemical separation membranes, Science 332 (2011) 674–676.
[16] J. Beenakker, V. Borman, S.Y. Krylov, Molecular transport in subnanometer pores: zero-point energy, reduced dimensionality and quantum sieving, Chem. Phys. Lett. 232 (1995) 379–382.
[17] A.A. Kumar, S.K. Bhatia, Quantum effect induced reverse kinetic molecular sieving in microporous materials, Phys. Rev. Lett. 95 (2005), 245901.
[18] A.A. Kumar, H. Jobic, S.K. Bhatia, Quantum effects on adsorption and diffusion of hydrogen and deuterium in microporous materials, J. Phys. Chem. B 110 (2006) 16666–16671.
[19] S.W. Rick, D. Lynch, J. Doll, The quantum dynamics of hydrogen and deuterium on the Pd (111) surface: a path integral transition state theory study, J. Chem. Phys. 99 (1993) 8183–8193.
[20] M. Pavese, G.A. Voth, Pseudopotentials for centroid molecular dynamics: application to self-diffusion in liquid para-hydrogen, Chem. Phys. Lett. 249 (1996) 231–236.
[21] S. Miura, S. Okazaki, K. Kinugawa, A path integral centroid molecular dynamics study of nonsuperfluid liquid helium-4, J. Chem. Phys. 110 (1999) 4523–4532.
[22] Q. Wang, S.R. Challa, D.S. Sholl, J.K. Johnson, Quantum sieving in carbon nanotubes and zeolites, Phys. Rev. Lett. 82 (1999) 956.
[23] S.R. Challa, D.S. Sholl, J.K. Johnson, Light isotope separation in carbon nanotubes through quantum molecular sieving, Phys. Rev. B 63 (2001), 245419.

[24] B. Hathorn, B. Sumpter, D. Noid, Contribution of restricted rotors to quantum sieving of hydrogen isotopes, Phys. Rev. 64 (2001), 022903.
[25] S.R. Challa, D.S. Sholl, J.K. Johnson, Adsorption and separation of hydrogen isotopes in carbon nanotubes: multicomponent grand canonical Monte Carlo simulations, J. Chem. Phys. 116 (2002) 814–824.
[26] T. Lu, E.M. Goldfield, S.K. Gray, The equilibrium constants for molecular hydrogen adsorption in carbon nanotubes based on iteratively determined nano-confined bound states, J. Theor. Comput. Chem. 2 (2003) 621–625.
[27] T. Lu, E.M. Goldfield, S.K. Gray, Quantum states of molecular hydrogen and its isotopes in single-walled carbon nanotubes, J. Phys. Chem. B 107 (2003) 12989–12995.
[28] L. Tun, E. Goldfield, S. Gray, Quantum states of molecular hydrogen and its isotopes in single-walled carbon nanotubes, J. Phys. Chem. B 107 (2003) 12989–12995.
[29] T.D. Hone, G.A. Voth, A centroid molecular dynamics study of liquid para-hydrogen and ortho-deuterium, J. Chem. Phys. 121 (2004) 6412–6422.
[30] G. Garberoglio, M.M. DeKlavon, J.K. Johnson, Quantum sieving in single-walled carbon nanotubes: effect of interaction potential and rotational– translational coupling, J. Phys. Chem. B 110 (2006) 1733–1741.
[31] T. Lu, E.M. Goldfield, S.K. Gray, Quantum states of hydrogen and its isotopes confined in single-walled carbon nanotubes: dependence on interaction potential and extreme two-dimensional confinement, J. Phys. Chem. B 110 (2006) 1742–1751.
[32] P. Kowalczyk, P.A. Gauden, A.P. Terzyk, S.K. Bhatia, Thermodynamics of hydrogen adsorption in slit-like carbon nanopores at 77 K. Classical versus path-integral Monte Carlo simulations, Langmuir 23 (2007) 3666–3672.
[33] A.A. Kumar, H. Jobic, S.K. Bhatia, Quantum effect induced kinetic molecular sieving of hydrogen and deuterium in microporous materials, Adsorption 13 (2007) 501–508.
[34] A.A. Kumar, S.K. Bhatia, Is kinetic molecular sieving of hydrogen isotopes feasible? J. Phys. Chem. C 112 (2008) 11421–11426.
[35] X. Zhao, S. Villar-Rodil, A.J. Fletcher, K.M. Thomas, Kinetic isotope effect for H2 and D2 quantum molecular sieving in adsorption/desorption on porous carbon materials, J. Phys. Chem. B 110 (2006) 9947–9955.
[36] H. Tanaka, H. Kanoh, M. Yudasaka, S. Iijima, K. Kaneko, Quantum effects on hydrogen isotope adsorption on single-wall carbon nanohorns, J. Am. Chem. Soc. 127 (2005) 7511–7516.
[37] Y. Hattori, H. Tanaka, F. Okino, H. Touhara, Y. Nakahigashi, S. Utsumi, H. Kanoh, K. Kaneko, Quantum sieving effect of modified activated carbon fibers on H2 and D2 adsorption at 20 K, J. Phys. Chem. B 110 (2006) 9764–9767.
[38] T. Nguyen, H. Jobic, S. Bhatia, Microscopic observation of kinetic molecular sieving of hydrogen isotopes in a nanoporous material, Phys. Rev. Lett. 105 (2010), 085901.
[39] M. Bieri, M. Treier, J. Cai, K. Aït-Mansour, P. Ruffieux, O. Gröning, P. Gröning, M. Kastler, R. Rieger, X. Feng, Porous graphenes: two-dimensional polymer synthesis with atomic precision, Chem. Commun. (2009) 6919–6921.
[40] S. Blankenburg, M. Bieri, R. Fasel, K. Müllen, C.A. Pignedoli, D. Passerone, Porous graphene as an atmospheric nanofilter, Small 6 (2010) 2266–2271.
[41] J. Schrier, Fluorinated and nanoporous graphene materials as sorbents for gas separations, ACS Appl. Mater. Interfaces 3 (2011) 4451–4458.
[42] H. Liu, V.R. Cooper, S. Dai, D.-e. Jiang, Windowed carbon nanotubes for efficient CO2 removal from natural gas, J. Phys. Chem. Lett. 3 (2012) 3343–3347.
[43] H.W. Kim, H.W. Yoon, S.-M. Yoon, B.M. Yoo, B.K. Ahn, Y.H. Cho, H.J. Shin, H. Yang, U. Paik, S. Kwon, Selective gas transport through few-layered graphene and graphene oxide membranes, Science 342 (2013) 91–95.
[44] R. Joshi, P. Carbone, F.-C. Wang, V.G. Kravets, Y. Su, I.V. Grigorieva, H. Wu, A. K. Geim, R.R. Nair, Precise and ultrafast molecular sieving through graphene oxide membranes, Science 343 (2014) 752–754.
[45] H. Liu, Z. Chen, S. Dai, D.-e. Jiang, Selectivity trend of gas separation through nanoporous graphene, J. Solid State Chem. 224 (2015) 2–6.
[46] H. Furukawa, O.M. Yaghi, Storage of hydrogen, methane, and carbon dioxide in highly porous covalent organic frameworks for clean energy applications, J. Am. Chem. Soc. 131 (2009) 8875–8883.
[47] A.P. Cote, A.I. Benin, N.W. Ockwig, M. O'Keeffe, A.J. Matzger, O.M. Yaghi, Porous, crystalline, covalent organic frameworks, Science 310 (2005) 1166–1170.
[48] E.L. Spitler, W.R. Dichtel, Lewis acid-catalysed formation of two-dimensional phthalocyanine covalent organic frameworks, Nat. Chem. 2 (2010) 672.
[49] X. Feng, X. Ding, D. Jiang, Covalent organic frameworks, Chem. Soc. Rev. 41 (2012) 6010–6022.
[50] J.W. Colson, W.R. Dichtel, Rationally synthesized two-dimensional polymers, Nat. Chem. 5 (2013) 453–465.
[51] X.-S. Wang, M. Chrzanowski, W.-Y. Gao, L. Wojtas, Y.-S. Chen, M.J. Zaworotko, S. Ma, Vertex-directed self-assembly of a high symmetry supermolecular building block using a custom-designed porphyrin, Chem. Sci. 3 (2012) 2823–2827.
[52] L. Latos-Grazynski, in: K.M. Kadish, K.M. Smith, R. Guilard (Eds.), The Porphyrin Handbook, Academic, New York, 2000.
[53] I. Gupta, M. Ravikanth, Recent developments in heteroporphyrins and their analogues, Coord. Chem. Rev. 250 (2006) 468–518.
[54] B. Szyszko, L. Latos-Grażyński, Core chemistry and skeletal rearrangements of porphyrinoids and metalloporphyrinoids, Chem. Soc. Rev. 44 (2015) 3588–3616.
[55] P.J. Chmielewski, L. Latos-Grażyński, Core modified porphyrins–a macrocyclic platform for organometallic chemistry, Coord. Chem. Rev. 249 (2005) 2510–2533.
[56] M. Broadhurst, R. Grigg, A. Johnson, Synthesis of porphin analogues containing furan and/or thiophen rings, J. Chem. Soc. C Org. (1971) 3681–3690.
[57] M. Broadhurst, R. Grigg, A. Johnson, 18-and 22-π-Electron macrocycles containing furan, pyrrole, and thiophen rings, J. Chem. Soc. D Chem. Commun. (1969) 1480–1482.
[58] M. Broadhurst, R. Grigg, A. Johnson, Preparation of some sulphur-containing polypyrrolic macrocycles. Sulphur extrusion from a meso-thiaphlorin, J. Chem. Soc. D Chem. Commun. (1970) 807–809.
[59] A. Tovmasyan, R.S. Sampaio, M.-K. Boss, J.C. Bueno-Janice, B.H. Bader, M. Thomas, J.S. Reboucas, M. Orr, J.D. Chandler, Y.-M. Go, Anticancer therapeutic potential of Mn porphyrin/ascorbate system, Free Radic. Biol. Med. 89 (2015) 1231–1247.
[60] B. Bui, L. Liu, W. Chen, Latex carrier for improving protoporphryin IX properties for photodynamic therapy, Photodiagnosis Photodyn. Ther. 14 (2016) 159–165.
[61] A.K. Mandal, J. Iqbal, A versatile aerobic oxidation of organic compounds catalyzed by cobalt (II) porphyrins, Tetrahedron 53 (1997) 7641–7648.
[62] Z. Tian, S. Dai, D.-e. Jiang, Expanded porphyrins as two-dimensional porous membranes for CO2 separation, ACS Appl. Mater. Interfaces 7 (2015) 13073–13079.
[63] T. Chatterjee, V.S. Shetti, R. Sharma, M. Ravikanth, Heteroatom-containing porphyrin analogues, Chem. Rev. 117 (2017) 3254–3328.
[64] K. Ayub, Transportation of hydrogen atom and molecule through X12Y12 nano-cages, Int. J. Hydrogen Energy 42 (2017) 11439–11451.
[65] S. Grimme, Semiempirical GGA-type density functional constructed with a long-range dispersion correction, J. Comput. Chem. 27 (2006) 1787–1799.
[66] C.A. Morgado, J.P. McNamara, I.H. Hillier, N.A. Burton, M.A. Vincent, Density functional and semiempirical molecular orbital methods including dispersion corrections for the accurate description of noncovalent interactions involving sulfur-containing molecules, J. Chem. Theor. Comput. 3 (2007) 1656–1664.
[67] Y. Zhao, D.G. Truhlar, Hybrid meta density functional theory methods for thermochemistry, thermochemical kinetics, and noncovalent interactions: the MPW1B95 and MPWB1K models and comparative assessments for hydrogen bonding and van der Waals interactions, J. Phys. Chem. 108 (2004) 6908–6918.
[68] Y. Zhao, D.G. Truhlar, Design of density functionals that are broadly accurate for thermochemistry, thermochemical kinetics, and nonbonded interactions, J. Phys. Chem. 109 (2005) 5656–5667.
[69] Y. Zhao, O. Tishchenko, D.G. Truhlar, How well can density functional methods describe hydrogen bonds to π acceptors? J. Phys. Chem. B 109 (2005) 19046–19051.
[70] Y. Zhao, M.T. Lusk, A.C. Dillon, M.J. Heben, S.B. Zhang, Boron-based organometallic nanostructures: hydrogen storage properties and structure stability, Nano Lett. 8 (2008) 157–161.
[71] Y. Zhao, D.G. Truhlar, The M06 suite of density functionals for main group thermochemistry, thermochemical kinetics, noncovalent interactions, excited states, and transition elements: two new functionals and systematic testing of four M06-class functionals and 12 other functionals, Theor. Chem. Acc. 120 (2008) 215–241.
[72] N. Kosar, S. Munsif, K. Ayub, T. Mahmood, Storage and permeation of hydrogen molecule, atom and ions (H+ and H−) through silicon carbide nanotube; a DFT approach, Int. J. Hydrogen Energy 46 (2021) 9163–9173.
[73] K. Ayub, Binding affinity and permeation of X12Y12 nanoclusters for helium and neon, J. Mol. Liq. 244 (2017) 124–134.
[74] A. Ayub, K. Ayub, S. Gul, M.A. Hashmi, A. Lakhani, S. Iqbal, J. Iqbal, Hetero-porphyrin based channel for separation of proton isotope: a density functional theory study, Microporous Mesoporous Mater. (2022), 111995.
[75] M. Miao, M.B. Nardelli, Q. Wang, Y. Liu, First principles study of the permeability of graphene to hydrogen atoms, Phys. Chem. Chem. Phys. 15 (2013) 16132–16137.
[76] Q. Zhang, M. Ju, L. Chen, X.C. Zeng, Differential permeability of proton isotopes through graphene and graphene analogue monolayer, J. Phys. Chem. Lett. 7 (2016) 3395–3400.
[77] Y. Feng, J. Chen, W. Fang, E.-G. Wang, A. Michaelides, X.-Z. Li, Hydrogenation facilitates proton transfer through two-dimensional honeycomb crystals, J. Phys. Chem. Lett. 8 (2017) 6009–6014.
[78] W.L. Wang, E. Kaxiras, Graphene hydrate: theoretical prediction of a new insulating form of graphene, New J. Phys. 12 (2010), 125012.
[79] I. Poltavsky, L. Zheng, M. Mortazavi, A. Tkatchenko, Quantum tunneling of thermal protons through pristine graphene, J. Chem. Phys. 148 (2018), 204707.
[80] M. Lozada-Hidalgo, S. Hu, O. Marshall, A. Mishchenko, A. Grigorenko, R. Dryfe, B. Radha, I. Grigorieva, A. Geim, Sieving hydrogen isotopes through two-dimensional crystals, Science 351 (2016) 68–70.